JOURNAL OF GEOPHYSICAL RESEARCH, VOL. 98, NO. B10, PAGES 17,911–17,920, OCTOBER 10, 1993

Fault Strain and Seismic Coupling on Mid-Ocean Ridges

PATIENCE A. COWIE,[1] CHRISTOPHER H. SCHOLZ,[2] MARGO EDWARDS,[3] AND ALBERTO MALINVERNO[4]

Lamont-Doherty Earth Observatory of Columbia University, Palisades, New York

The contribution of extensional faulting to seafloor spreading along the East Pacific Rise (EPR) axis near 3°S and between 13°N and 15°N is calculated using data on the displacement and length distributions of faults obtained from side scan sonar and bathymetric data. It is found that faulting may account for of the order of 5-10% of the total spreading rate, which is comparable to a previous estimate from the EPR near 19°S. Given the paucity of normal faulting earthquakes on the EPR axis, a maximum estimate of the seismic moment release shows that seismicity can account for only 1% of the strain due to faulting. This result leads us to conclude that most of the slip on active faults must be occurring by stable sliding. Laboratory observations of the stability of frictional sliding show that increasing normal stress promotes unstable sliding, while increasing temperature promotes stable sliding. By applying a simple frictional model to mid-ocean ridge faults it is shown that at fast spreading ridges (≥90 mm/yr) the seismic portion of a fault (W_s) is a small proportion of the total downdip width of the fault (W_f). The ratio W_s/W_f is interpreted as the seismic coupling coefficient χ, and in this case $\chi \approx 0$. In contrast, at slow spreading rates (≤40 mm/yr), $W_s \approx W_f$, and therefore $\chi \approx 1$, which is consistent with the occurrence of large-magnitude earthquakes (m_b= 5.0 to 6.0) occurring, for example, along the Mid-Atlantic Ridge axis.

INTRODUCTION

The use of high-resolution sonar mapping systems in the ocean basins has revealed a pervasive fabric of normal faults that dissect the seafloor at mid-ocean ridges [*Edwards et al.*, 1991, *Carbotte and Macdonald,* 1990; *Kong et al.*, 1988; *Bicknell et al.*, 1987; *Crane*, 1987; *Searle*, 1984; *Laughton and Searle*, 1979; *Macdonald and Atwater*, 1978; *Macdonald and Lyendyk*, 1977; *Lonsdale*, 1977; *Lonsdale and Spiess*, 1980; *Klitgord and Mudie*, 1974]. These faults develop in a narrow zone at the ridge axis in response to extension, and as seafloor spreading proceeds they become inactive and are preserved as irregular topography on the ridge flanks. The fossil fault population on the ridge flanks therefore represents the extensional strain achieved in the active tectonic zone.

The contribution of fault strain to plate separation at slow spreading ridges has been estimated by summing the seismic moments of normal faulting earthquakes occurring at the ridge axis [*Solomon et al.*, 1988]. Solomon et al. calculated that seismic faulting could account for 10% to 20% of the total spreading rate for spreading rates ≤40 mm/yr. However, at fast spreading centers (>90 mm/yr) most of the earthquakes that have been detected occur in swarms of low magnitude events usually associated with hydrothermal circulation and/or magmatic intrusions [*Riedesel et al.*, 1982; *Macdonald and Mudie*, 1974]. More recently *Wilcock et al.* [1992] documented microearthquake activity associated with faulting on the East Pacific Rise (EPR) but this activity is restricted to the region of the overlapping spreading center near 9°N. The spreading centers of the EPR are virtually aseismic above the teleseismic detection threshold which generally lies in the range m_b = 4.0-5.0 in this geographic area [*Riedesel et al.*, 1982]. The teleseismic observations do not preclude seismicity occurring below this threshold, but large-magnitude earthquakes in this area are generally either strike-slip events along transform faults [e.g., *Kawasaki et al.*, 1985] or intraplate events in young ocean lithosphere [*Wiens and Stein*, 1984]. However, although seismic deformation appears to make a negligible contribution to extension at fast spreading centers, the abundant scarps of normal faults seen on sonar images of the seafloor testify that faulting does play a significant role in the process of seafloor spreading and deformation of oceanic crust at all spreading rates [*Rea*, 1975; *Searle*, 1984; *Macdonald and Luyendyk*, 1985; *Carbotte and Macdonald*, 1990; *Malinverno*, 1991; *Malinverno and Cowie*, this issue].

The purpose of this paper is to calculate the extensional strain represented by the fault scarps preserved on the flanks of the EPR and to compare it with a hypothetical estimate of the seismic moment release rate assuming no limitation to earthquake detection. The strain estimates obtained from the fault population represent the total brittle strain, i.e., both seismic and aseismic. From these calculations we can therefore determine the ratio of seismic to aseismic deformation, which is a measure of the seismic coupling of the faults. *Bicknell et al.* [1987] estimated the percentage fault strain on the EPR at 19°S by adding up the displacement on faults imaged along a 110-km-long high-resolution ridge-perpendicular bathymetric profile. Bicknell et al. estimated a fault strain of 5.3% (4.2% on the Nazca plate; 6.4% on the Pacific plate). The method of summing fault displacements in a cross section assumes that all the faults extend to infinity along strike. While this assumption is valid for the case of perfect two-dimensional strain, which may seem a reasonable approximation for a mid-ocean ridge, a reliable strain estimate requires several lines to be measured and an average value to be determined. The approach used here, derived from the work of *Kostrov* [1974], does not rely on the assumption of two-dimensionality because it uses information on both the

[1] Now at Department of Geology and Geophysics, Edinburgh University, Edinburgh, Scotland.
[2] Also at the Department of Geological Sciences, Columbia University, New York.
[3] Now at SOEST, University of Hawaii at Manoa, Honolulu, Hawaii.
[4] Now at Schlumberger-Doll Research, Ridgefield, Connecticut.

Paper number 93JB01567.
0148-0227/93/93JB-01567$05.00

lengths and the displacements of all the faults. The total fault strain is the sum of the geometric moments of all the faults in a deformed volume, where geometric moment is the displacement on a fault multiplied by its surface area.

Summing the geometric moments for a large number of faults is simplified, in this study, by using a scaling relationship between the displacement on a fault and its length [*Scholz and Cowie*, 1990]. A displacement-length scaling relationship has already been demonstrated for faults in continental areas [*Cowie and Scholz*, 1992*a*]. This relationship is established near 3°S on the EPR by correlating faults scarps identified in a ridge-perpendicular bathymetric profile with a fault lineation map produced from side scan sonar images. The strain estimates depend on the completeness of the data set for small-scale faulting which is a function of the resolution of the mapping system used. We show here how the effect of limited system resolution can be estimated by using a functional form for the distribution of fault lengths and assuming the distribution can be extrapolated to sub-resolution-scale faulting. In this study, we have analyzed the length distributions of faults on the flanks of the EPR between 13°N and 15°N and near 3°S using data from side scan sonar images.

The disparity between the calculated fault strain and the seismic moment release on the EPR is discussed in the context of a frictional model for faults at mid-ocean ridges. The model is derived from laboratory observations of the stability of frictional sliding; a model similar to that presented here has already been considered for continental faults [*Tse and Rice*, 1986; *Scholz*, 1988*a*]. In this model, the portion of the fault that can slide unstably, and thus produce earthquakes, is determined by the position of frictional stability transitions which are controlled by the stress and thermal regimes at the ridge axis. The model predicts that slip on active normal faults at fast spreading ridges is occurring by stable, as opposed to stick-slip, sliding due to the high geothermal gradient. Stable sliding on faults may be associated with low-level seismicity, as it is along the creeping section of the San Andreas fault in central California, but in this case the seismicity represents a small proportion of the total slip occurring on the fault [*Scholz*, 1990, p. 312].

STRAIN CALCULATION

From *Kostrov* [1974] the amount of strain represented by a population of faults can be calculated using

$$\varepsilon_{ij} = \frac{1}{2V}\sum_{k=1}^{N_T}[M_{ij}]_k \tag{1}$$

where N_T is the total number of faults in the population and V is the size of the faulted volume. M_{ij} is the geometric moment of each fault which is given by

$$M_{ij} = M_o\,(\delta_i n_j + n_i \delta_j) \tag{2}$$

where δ is a unit vector which defines the sense of displacement on the fault, and $\boldsymbol{n}$ is a unit vector normal to the fault plane. M_o is the magnitude of the geometric moment and is given by

$$M_o = d\,L\,W_f \tag{3}$$

where L is the mapped length of the fault trace, W_f is its downdip extent, and d is the displacement on the fault. The maximum depth of faulting, t, is the depth of the transition from predominantly brittle deformation in the upper part of the crust to ductile deformation at greater depth. Large faults that break all the way through the brittle layer grow by increasing their length while their width W_f remains constant, i.e., $W_f = t/\sin(\theta)$ (Figure 1). For small faults with lengths less than the dimension t, the fault surface is approximately equidimensional so that $W_f \approx L$. The size of the faulted volume V is given by

$$V = A\,t \tag{4}$$

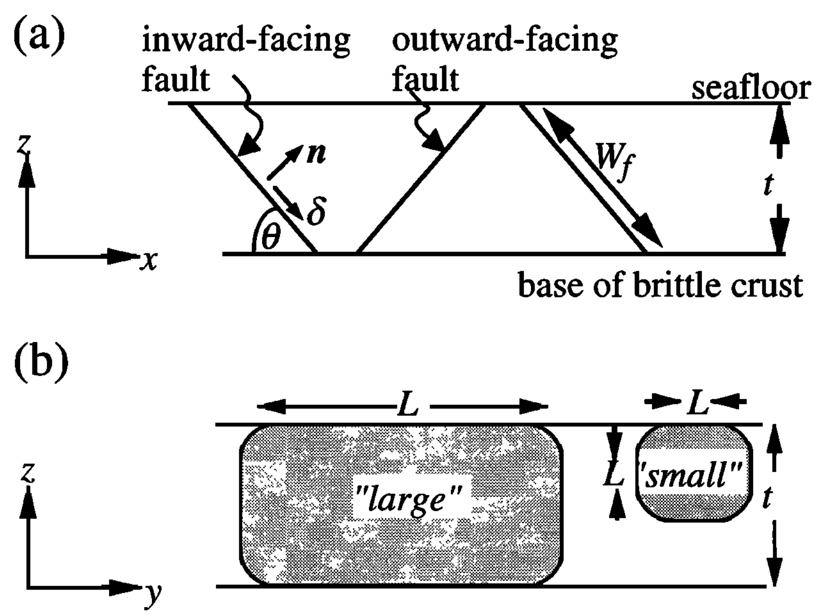

FIG. 1 (*a*) Simplified model for normal faulting at the rise axis showing the parameters used in the strain calculation: θ is the dip of the faults; t is the thickness of the faulted upper portion of the crust; W_f is the fault dimension measured downdip in the plane of the fault. (*b*) Simplified view of "small faults", which break through only a portion of the brittle crust and grow in both strike and downdip directions, and "large faults" which grow only in their length dimension.

where A is the areal extent of the faults used in the strain calculation. An upper estimate of the total strain is obtained if we assume $A = D\, L_{max}$, where D is the width of the deformed region measured perpendicular to the ridge axis and L_{max} is the length of the longest fault. This value for A implies that at the scale of the largest fault the strain is two-dimensional (and just equal to the displacement on this fault normalized by D); faults shorter than L_{max} contribute a strain scaled by the ratio L/L_{max}. If, alternatively, we use A equal to the size of survey area in equation (4), then the value of A is arbitrary. In other words, in this latter case we are implicitly assuming that an increase in the extent of the survey would increase, by the same proportion, the numbers of faults of all sizes found in that area. This may be the case for shorter faults, but the largest faults, which represent most of the strain, will tend to be under represented (e.g., they might extend out of the area) unless the survey area increases in multiples of L_{max}. Consequently, using the survey area in the calculation will generally give a lower strain estimate. We calculate both upper ($A = D\, L_{max}$) and lower estimates (A = survey area). If the faults dip at an angle θ (Figure 1), then for faults that dip away from the axis (outward facing faults) the vectors $\boldsymbol{\delta}$ and $\boldsymbol{n}$ are

$$\begin{aligned} \boldsymbol{n} &= (\sin(\theta), 0, \cos(\theta)), \\ \boldsymbol{\delta} &= (\cos(\theta), 0, -\sin(\theta)) \end{aligned} \tag{5a}$$

while for faults that dip toward the axis (inward facing faults),

$$\begin{aligned} \boldsymbol{n} &= (-\sin(\theta), 0, \cos(\theta)), \\ \boldsymbol{\delta} &= (-\cos(\theta), 0, -\sin(\theta)). \end{aligned} \tag{5b}$$

The only nonzero terms in equation (2) are M_{xx} (ridge-perpendicular deformation) and M_{zz} (crustal thickness changes). We assume that both inward and outward facing faults have the same dip and are parallel to the ridge axis. This assumption is clearly an oversimplification but there is insufficient data available to argue for systematic variations in θ. For a fixed value of θ, M_{xx} and M_{zz} are the same for both fault sets. From equation (1), the extensional strain ε_{xx} perpendicular to the ridge crest, due to both inward and outward facing faults, is

$$\varepsilon_{xx} = \frac{\cos(\theta)}{A} \sum_{k=1}^{N_T} d_k L_k \tag{6a}$$

for large faults ($L \geq t$). For small faults ($L \leq t$), ε_{xx} is

$$\varepsilon_{xx} = \frac{\cos(\theta)\sin(\theta)}{A\, t} \sum_{k=1}^{N_T} d_k (L_k)^2 \tag{6b}$$

Note that specifying the maximum depth of faulting, t, defines the limit of the large fault population and is necessary for calculating the contribution of small faults (equation (6b)).

Equations 6a and 6b may be reduced to summations of fault lengths alone if the relationship between the displacement on a fault, d, and its length L is known. The usefulness of such a displacement-length scaling relationship is that the strain may then be calculated from information on fault lengths alone [*Scholz and Cowie*, 1990]. *Cowie and Scholz* [1992a, b] argued that for continental faults the relationship between the maximum displacement on a fault and its length is linear:

$$d = \gamma L \tag{7}$$

where γ is a constant that depends on the rock type and the tectonic environment in which the faults form. *Gillespie et al.* [1992] argued that the relationship is nonlinear if many fault data sets from different regions and rock types are combined. The validity of a linear relationship given by equation (7) for normal faults on the EPR is investigated in this study and discussed in detail below.

If the distribution of fault lengths has a functional form, we can write $N(L_1, L_2)$ the number of faults of length between L_1 and L_2 as

$$N(L_1, L_2) = N_T \int_{L_1}^{L_2} f(L)\, dL \tag{8}$$

where N_T is the total number of faults, and $f(L)$ is the probability density function of the fault lengths. In this case, the summation in equation (6) can be reduced to an integration that can be solved analytically. Although the integral method uses an idealized (e.g., best fit) length distribution, it has the advantage that the sensitivity of the strain calculation to the resolution limit of the data set can also be investigated. For example, substituting equations (7) and (8) into equation (6), the equivalent integral expressions are

$$\varepsilon_{xx} = \frac{\gamma \cos(\theta)\, N_T}{A} \int_t^{L_{max}} f(L)\, L^2\, dL \tag{9a}$$

for large faults ($L_{max} > t$), and for small faults,

$$\varepsilon_{xx} = \frac{\gamma \cos(\theta) \sin(\theta)\, N_T}{A\, t} \int_{L_{min}}^{t} f(L)\, L^3\, dL \tag{9b}$$

where L_{max} is the longest fault and L_{min} is the shortest fault resolved in the data set. Using equation (9), we can investigate the sensitivity of our strain estimates to the value of L_{min}, as L_{min} tends to zero.

FAULT PARAMETERS

Length Distribution

The lengths of faults were obtained from side scan sonar images collected on the EPR using the SeaMARC II mapping system between 13°N and 15°N [see *Edwards et al.*, 1989, 1991] and the GLORIA (Geological LOng Range Inclined Asdic) mapping system near 3°S [see *Searle*, 1984]. The SeaMARC II device images the seafloor using 12 kHz sound waves and covers a 10-km-wide swath with an across-track resolution of 5 m [*Blackinton et al.*, 1983]. By comparison, GLORIA is a lower-resolution system; the Mark II version operates at a frequency of about 6 kHz and covers a swath that is up to 60 km wide with an across-track resolution of about 30 m [*Laughton*, 1981; *Tyce*, 1986]. For the area between 13°N and 15°N the lengths were measured from a fault trace map at a scale of 1:200,000 using digital SeaMARC II images displayed at a 50-m pixel resolution. The fault length data for the area at 3°S on the EPR were compiled from analog GLORIA images at a scale of 1:270,000. In the fault length interpretation we took into consideration the fact that the SeaMARC II data were collected along survey lines oriented at 45° to the fault fabric whereas the GLORIA data were collected along fault-parallel survey lines. Oblique survey lines make lineation mapping across adjacent swaths more subjective and less sensitive to structural detail whereas fault-parallel lines highlight structural discontinuities in the fault traces. Moreover, the GLORIA survey imaged inward and outward facing fault populations separately. In the SeaMARC II interpretation we found that the longer faults actually consist of several segments and often the facing direction of segments can change along strike. Therefore in order to compare the two data sets, we recombined the inward and outward facing fault populations interpreted from the GLORIA images. We also applied a criterion that segments offset by ≤ 150 m belong to the same fault system. Note that the resolution limit of the SeaMARC II swath images used for the analysis between 13°N and 15°N is about 140 m (= $2(2)^{1/2}$(pixel size)), so that offsets of this size or smaller cannot be easily resolved. This scale is also comparable to the size of discontinuities along normal faults mapped in Iceland [*Gudmundsson*, 1987*a*, *b*].

Figure 2*a* shows the cumulative distributions of fault lengths for the two study areas. Both distributions are best described by the function

$$N_L = N_T \exp(-\lambda L) \qquad (10)$$

where N_L is the number of faults with length $\geq L$ and λ is the reciprocal of the mean fault length $\langle L \rangle$. The slope of the best-fit straight line through the data plotted on log linear axes gives the value of λ, which is listed in Table 1. The probability density function corresponding to (10) is $f(L) = \lambda \exp(-\lambda L)$.

Displacement-Length Coefficient γ

In general, the displacement profile along the trace of a fault can be described as bell-shaped or elliptical. The maximum value occurs toward the center of the profile. The displacement is fairly constant over at least the central third of the fault trace and then dies out to zero at the fault tips. A linear correlation between the displacement on a fault and its length has been demonstrated by *Cowie and Scholz* [1992*a*] for continental faults. They show that the ratio of maximum displacement to length (which is the parameter γ) ranges between approximately 5.0×10^{-3} and 6.0×10^{-2} depending on the tectonic setting and rock type in which the faults form [*Cowie and Scholz*, 1992*b*].

To construct the displacement-length scaling relationship for the faults near 3°S the lengths were measured directly from the GLORIA side scan images (see above). The fault displacements were determined by measuring fault scarp heights along a ridge-perpendicular bathymetric profile in the same area (taken from [*Lonsdale* [1977]). This profile was obtained using the high-resolution Scripps Institute deep-tow tool which has an effective vertical resolution of a few meters [*Lonsdale*, 1977; *Kleinrock et al.*, 1992]. The scarp heights were converted to a displacement by assuming the dip of the faults (45° in this case). We also implicitly assumed in this conversion that the actual offset across the fault is reflected in the bathymetry, i.e, that sediment infilling adjacent to the fault may be neglected. The measurements were corrected to allow for the fact that the bathymetric line does not always intersect the fault where the displacement is at its maximum value. To do this we assumed that at a point x from the mid-point of the fault trace the displacement is given by $d_{max}(1 - (x/L)^2)^{1/2}$. The values of the ratio γ range from about 2.5×10^{-3} to about 1.7×10^{-2} with a mean value of $6.7 \times 10^{-3} \pm 2.0 \times 10^{-3}$. The scatter in the data shown in Figure 2*b* is typical of that observed in continental fault data sets, and *Cowie and Scholz* [1992*a*] attribute this variation to both the process of fault development and data collection procedures. S. M. Carbotte and K. C. Macdonald (Comparison of seafloor tectonic fabric at intermediate, fast, and ultrafast spreading ridges, submitted to *Journal of Geophysical Research*, 1993) found a value for γ of $8.1 \times 10^{-3} \pm 0.8 \times 10^{-3}$ by correlating fault scarps observed along a deep-tow line published by *Lonsdale and Spiess* [1977] with SeaMARC II fault lineation mapping near 9°N on the EPR.

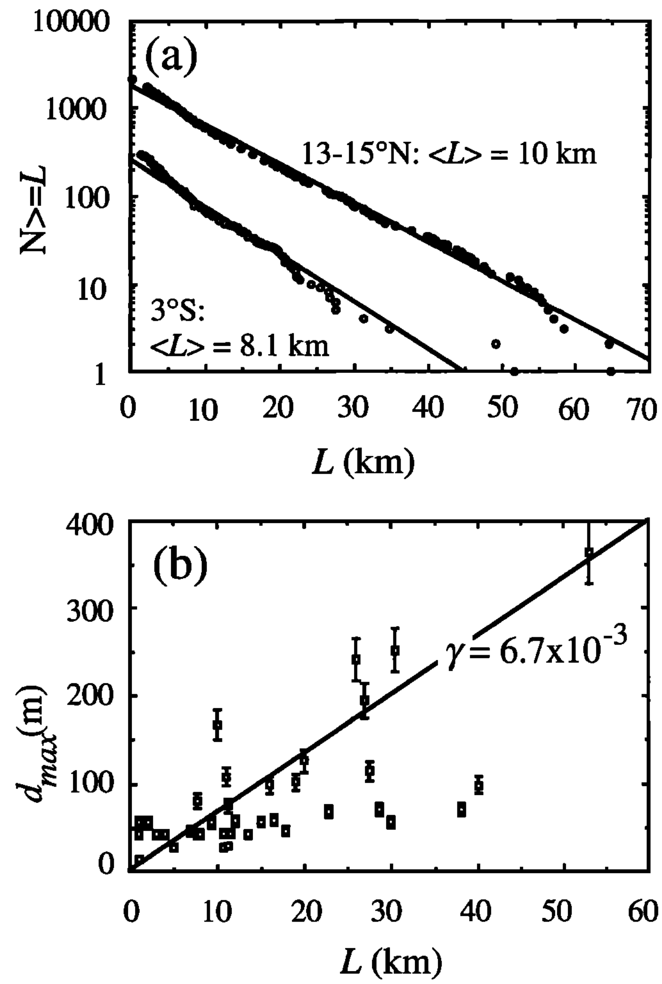

FIG. 2. (*a*) Cumulative distributions of fault lengths obtained from SeaMARC II images at 13°-15°N (dots) and from GLORIA images near 3°S (circles). The vertical axis is the number of faults with length ≥*L*. The slope of the distribution equals the reciprocal mean fault length <*L*>. (*b*) Displacement-length correlation plot for faults near 3°S. The maximum displacement is plotted and is calculated by assuming an elliptical displacement profile with the maximum displacement at the fault midpoint and zero displacement at the fault tips (see text for explanation). The error bars represent 10% uncertainty in the displacement estimates. The value for γ is also shown (equation 7).

STRAIN ESTIMATES

Strain estimates have been calculated for the areas near 3°S and between 13°N and 15°N using both the summation expression (equation (6) with $d = \gamma L$) and the integration expression (equation (9)) using the parameters listed in Table

TABLE 1. Summary of Fault Parameters and Strain Estimates

Location	Spreading Rate mm/yr	λ 1/km	L_{max} km	L_{surv} km	D km	Percent Strain	Method
19°S EPR	160				90	4.2-6.4	sum-$d^{\dagger}$
					70	8.9	sum-d
3°S EPR	152		53	75	65	3.4-5.2	sum-L
		0.12	45*	75	65	3.8-5.0	int-L
13°-15°N EPR	94		65	210	150	4.8-15.5	sum-L
		0.10	75*	210	150	5.1-14.2	int-L
37°N MAR	20					11-20	sum-$d^{\S}$

Here λ is the reciprocal mean fault length; L_{max} is the maximum measured fault length; L_{surv} is the length of the survey area measured parallel to the ridge axis; D is the width of the survey area measured perpendicular to the ridge axis. In last column, "sum-d" means the strain was calculated by summing fault displacements along a bathymetric profile; "sum-L" means that the actual measured fault lengths were summed, i.e. ΣL^2; "int-L" means that the best fit length distribution (equation 10) was used to calculate the strain using equation (9) and assuming L_{min} = 0. The lower strain estimate in the range (column 7) corresponds to $A = DL_{surv}$; the largest value corresponds to $A = DL_{max}$. EPR is East Pacific Rise, and MAR is Mid-Atlantic Ridge.

* This is the best fit value.

§ Values taken from *Macdonald and Luyendyk* [1977].

† Values taken from *Bicknell et al.* [1987].

1. A fault dip $\theta = 45°$ and a value for γ of $6.7\text{x}10^{-3}$ was assumed in all the calculations. Upper and lower estimates respectively were obtained depending on whether $A = D\,L_{max}$ or $A = D\,L_{surv}$, where L_{surv} is the length of the survey measured parallel to the faults. We use a value for t, the maximum depth to which faulting can occur, of 6 km. As previously mentioned, the value of t effects the amount of strain attributed to faults with length less than or equal to t. The contribution of small faults to the total fault strain has been estimated and is shown in Figure 3. Figure 3 shows the percentage of total fault strain accounted for plotted against the value of L_{min} for the parameters listed in Table 1, where L_{min} is the smallest fault that can be resolved in the data set. As L_{min} tends to zero the amount of fault strain accounted for approaches 100%. It is clear from Figure 3 that even if the data set is not complete for faults less than a few kilometers in length (i.e., $L \leq t$), these faults contribute a small proportion (<10%) of the total strain. Note that because the distribution of fault lengths is exponential (equation (10)) the strain converges more rapidly than it does for a power law distribution which characterizes continental fault populations [*Scholz and Cowie*, 1990; *Walsh et al.*, 1991]. The difference between the curves plotted in Figure 3 reflects the difference in the value of L_{max} in the two data sets. If L_{max} is not much greater than L_{min}, then the rate of convergence of the strain estimate is slow, i.e., the strain estimate is more sensitive to the resolution limit.

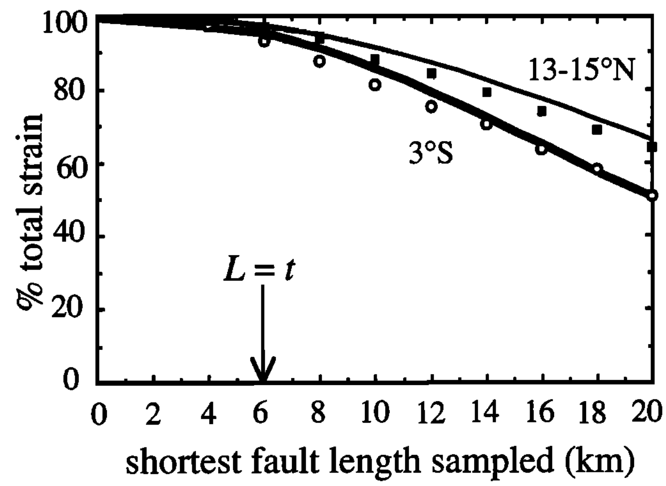

FIG. 3. Percentage of total fault strain as a function of the resolution limit for the area between 13°N and 15°N (thin line and squares) and the area near 3°S (bold line and circles). The lines were obtained using equation (9) with the best fit length length distribution functions. The points were obtained by summing the actual measured fault lengths in each case (equation (6) with $d = \gamma L$).

From examination of equations (6) and (9) it is evident that the values of the parameters γ and θ will have a significant effect on the magnitude of the strain estimate, yet these are also the parameters that are least well constrained. For example, if a fault dip of 60° instead of 45° is used, then the estimate of strain decreases by 30%. Similarly, a factor of 2 uncertainty in γ introduces a factor of 2 uncertainty in the strain estimate.

In Table 1 the upper estimate of strain for the area near 3°S ranges from 5.0 to 5.2% which is slightly lower than the value (8.9%) obtained by summing displacements along the deep-tow bathymetric profile. The upper strain estimate for the region between 13°N and 15°N is 14.2-15.5%. Using the size of the survey area in the calculations provides lower estimates of 3.4 to 3.8% at 3°S and 4.8-5.1% at 13°-15°N. The mean values of these two extremes are: 4.4% at 3°S and 10% between 13°N and 15°N. There is a large variability in these results and the range includes the estimates of 4.2% and 6.4% obtained by *Bicknell et al.* [1987] for the area near 19°S. S. M. Carbotte and K. C. Macdonald (submitted manuscript, 1993) calculated a strain of 3.1% for the area between 8°30'N and 10°N on the EPR and 4.5% for the area between 18°S and 19°S using fault data from SeaMARC II images for a fault dip of 45° and $\gamma = 8.1\times10^{-3}$. Note that Carbotte and Macdonald used the size of the survey area in these calculations so their results represent lower estimates.

Given the uncertainties in the calculation parameters, we can only conservatively conclude that brittle strain along the EPR axis is of the order of 5 to 10%, with a possible range from 3 to 15%. In contrast, the only measurement obtained directly from fault data at the slow spreading Mid-Atlantic Ridge (MAR) is in the range 10-20%. This measurement, from the MAR at 37°N where the spreading rate is 20 mm/yr, was made by *Macdonald and Luyendyk* [1977], who summed fault throws along a deep-tow bathymetric profile. This range for the MAR allows for a factor of 2 variation but, in comparison with the estimates along the EPR obtained here, our results suggest that the strain due to faulting is greater at slow spreading ridges. *Malinverno and Cowie* [this issue] reached a similar conclusion from a comparison of topographic roughness on the EPR and MAR assuming that all the roughness is due to faulting. An inverse relationship between fault strain and spreading rate can be argued, at least to first order, from the results of this study of the EPR: for spreading rates ≥150 mm/yr, $\varepsilon_{xx} \approx$ 3-9%; for spreading rates ≈ 100 mm/yr, $\varepsilon_{xx} \approx$ 5-15%.

SEISMICITY

In this study we reexamined the Harvard Centroid Moment Tensor (CMT) catalogue and the Bulletin of the International Seismological Centre (ISC) for the region of the EPR between 20°S and 30°N. It is difficult to evaluate unequivocally the seismic activity in this area because of poor station control due to the remoteness of continental seismic networks. Furthermore, the CMT catalogue is restricted to only the largest earthquakes worldwide (usually $m_b \geq 5.0$) with good station control and which occurred during the last 15 years or so. The CMT catalogue does have the advantage that it provides an estimate of the earthquake focal mechanism. CMT solutions in this region are primarily located on transform faults with focal mechanisms consistent with strike-slip motion. The ISC Bulletin indicates a number of additional earthquakes in the area during the last 30 years or so with magnitudes as low as $m_b = 3.5$ and which are scattered up to distances of a few hundred kilometers from the ridge axis. The magnitudes of these events are typically quite well constrained, particularly for the largest events (≤ ±0.2 magnitude units), but the location deteriorates rapidly with decreasing magnitude. For example, according to the ISC Bulletin, for $m_b \geq 5.0$ the location error is of the order of only ±5 km, whereas for $4.5 \leq m_b \leq 5.0$ the error is about ±20 km and for $4.0 \leq m_b \leq 4.5$ it is about ±50 km. *Wiens and Stein* [1984] and *Wysession et al.* [1991] identified a small number of large earthquakes ($m_b >\sim 5.0$) in this area which they classified as intraplate due to their distance from the plate boundary. Otherwise, the largest ISC events approximately colocate with the CMT solutions in this area, i.e., on transform faults. The majority of the smaller events are located less than 150 km from a transform fault. Therefore, given the uncertainty in their locations, it is possible that many of the smaller events may also be transform fault earthquakes.

On-site seismic studies of fast spreading ridges (for example, the Galapagos ridge [*Macdonald and Mudie*, 1974] and the EPR at 21°N [*Riedesel et al.*, 1982]) have found that the earthquake activity occurs in swarms of low-magnitude events ($m_b \leq 1.0$) more consistent with volcanic and hydrothermal activity than faulting. More recently, *Wilcock et al.* [1992] monitored microearthquakes at the overlapping spreading center near 9°N on the EPR. These workers interpret the earthquakes they observed as normal faulting events. The average earthquake magnitude measured was about m_b = 2.0-3.0; however, all the events were restricted to the vicinity of the overlapping spreading center itself, and none of the earthquakes recorded were otherwise located on the rise axis.

The seismicity data from the EPR do not entirely preclude earthquake activity associated with normal faulting along the spreading centers if the magnitude level of the seismicity is below the teleseismic detection threshold. Consequently, it is of interest here to present the calculation of a hypothetical seismic moment release rate at the ridge axis assuming there are no restrictions imposed by detection capabilities. To obtain a maximum estimate we assume that the largest normal faulting event on the EPR that has occurred within the 30 year period of the ISC catalogue has a magnitude 5.0, i.e., equal to the detection threshold, and that the seismicity below this threshold is distributed according to the global moment-frequency distribution with a power law exponent B equal to 0.6 (equivalent to the Gutenberg-Richter b value equal to 1.0). An earthquake of magnitude 5.0 has a mean slip of a few centimeters, a source radius of the order of a few kilometers, and a seismic moment of about 1.0×10^{17} N m. Integrating over the distribution of earthquakes, the total moment released by all the earthquakes is about 2 times that released by the largest earthquake [e.g., *Wesnousky et al.*, 1983, equation 4]. Over a 30-year time period therefore the seismicity accounts for a moment release rate of about 3×10^{15} (N m/yr. Seismic strain rate $\dot{\varepsilon}_s$ is related to moment release rate $\dot{M}_o$ according to $\dot{\varepsilon}_s = \dot{M}_o/(2\mu V)$, where μ is the shear modulus [e.g., *Ekstrom and England*, 1989]. The half width of the fault generation zone at the EPR axis is approximately 5 km (see *Edwards et al.*, [1991] for discussion); the thickness of the crust is 6 km; 50 km is taken as the maximum fault length L_{max}, giving V = 1500 km^3. Therefore, if $\mu = 3.0\times10^{11}$ N m^{-2} is used, the seismic strain rate is 4×10^{-9} year^{-1}. At a half spreading rate of 50 mm/year, a fault may be active for about 100,000 years before it moves out of the fault generation zone. The total seismic moment released over this time period produces a strain of 0.04% which is 2 orders of magnitude less than the calculated total fault strain along the EPR (see Table 1). In order for the seismicity to account for a significantly larger strain while remaining below the teleseismic detection threshold, there would have to be a high level of microearthquake activity (e.g., a B value close to 1.0) which has yet to be observed in ocean bottom seismic observations on mid-ocean ridges.

In contrast to the EPR, the CMT catalogue for the Mid-Atlantic Ridge shows many large-magnitude normal faulting events (m_b = 5.0-6.0) located on the spreading centers [*Huang and Solomon*, 1988]. By summing moments for earthquakes on slow spreading ridges, *Solomon et al.* [1988] showed that seismicity can account for 10-20% of the plate separation rate on slow spreading ridges. This is comparable to the estimates of fault strain calculated by *Macdonald and Luyendyk* [1977], using a deep-tow bathymetric profile across the MAR near 37°N, and by *Malinverno and Cowie* [this issue] from seafloor topographic roughness. However, there is only one direct estimate of strain from the MAR, and it may be quite variable along different portions of the ridge axis [e.g., *Shaw*, 1992].

DISCUSSION

Figure 4 shows a summary of the estimates of brittle deformation from both seismicity data and fault data for fast and slow spreading ridges. Plate separation at all spreading rates is clearly dominated by magmatic processes that create new crust, but a proportion of the total plate separation is accounted for by the formation of normal faults at the axis. According to these and previous calculations the contribution of faulting may be as much as 10-20% at slow spreading ridges and perhaps a factor of 2 lower (5-10%) at fast spreading ridges. There is, however, a much greater difference between the seismic activity associated with the faulting. Whereas the seismic moment release rate at slow spreading ridges appears to be similar to the brittle strain rate calculated from the fault population, at fast spreading ridges an upper estimate of the seismic moment release rate can only account for perhaps 1% of the strain represented by the faults.

Here we show that the fundamental variation in seismic activity with spreading rate of mid-ocean ridge normal faults can be explained by a model similar to that of *Tse and Rice* [1986], and discussed by *Scholz* [1988*a*], for the stability of frictional sliding on continental faults. This model is based on the idea that the part of the fault that can slip unstably and produce earthquakes is controlled by the position of frictional stability transitions and may be only a small part of the whole fault. The upper transition T_u is the depth at which sliding first becomes unstable in the shallow part of the crust and has, in the past, been attributed to the stabilizing effects of low normal stress or pore fluid effects. The lower transition T_l is where sliding can again occur by stable slip, by processes usually attributed to elevated temperatures and the onset of ductile deformation mechanisms.

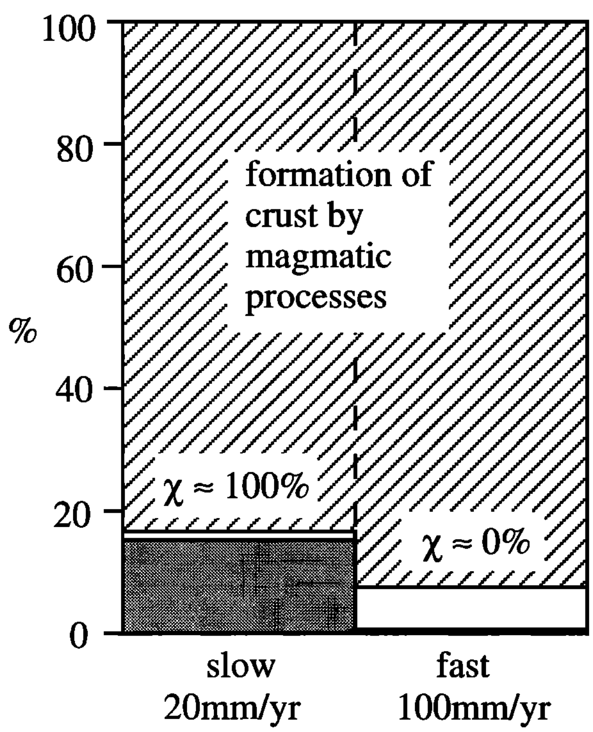

FIG. 4. Summary diagram comparing the partitioning between magmatic activity (hatched pattern), aseismic fault strain (white), and seismic fault strain (shaded) during seafloor spreading at fast and slow spreading ridges. The seismic coupling χ is a measure of the ratio of seismic strain to total (seismic plus aseismic) brittle strain (see text for discussion).

The stability of frictional sliding depends on three factors, the first being the critical slip distance l_c, which is the distance two surfaces in contact must slide, upon a velocity perturbation, for friction to change from a static to a dynamic value. The second factor is defined by the difference between two empirical constants (a - b), determined from laboratory friction experiments, which is the change in the steady state frictional resistance with sliding velocity. If the frictional resistance decreases with increasing velocity, then an instability occurs. If (a - b) is positive, sliding is intrinsically stable; if (a - b) is negative, sliding may be stable or unstable depending on the third factor, which is the stiffness of the sliding system. See *Scholz* [1990, p. 86] for discussion of this topic.

Tse and Rice [1986] showed that for continental strike-slip faults the lower stability transition T_l is the depth at which (a - b) changes from a negative to a positive value with increasing temperature. Therefore T_l depends on the geothermal gradient, and it approximately coincides with the transition from predominantly brittle deformation in the upper crust to ductile flow at greater depths in the crust. From the thermal models of *Lin and Parmentier* [1989] we estimated a geothermal gradient in the fault generation zone by averaging the gradients calculated at distances of 1 km and 5 km from the axis. For a fast spreading ridge (100 mm/yr full spreading rate) the average geothermal gradient is approximately 200°C/km, whereas on a slow spreading ridge (20 mm/yr full spreading rate) the average gradient is approximately 100°C/km (see Figure 5). Although the exact relationship between T_l and the brittle-ductile transition is not well defined, *Wiens and Stein* [1984] showed that according to a simple plate cooling model, seismicity in the oceans is confined to temperatures lower than approximately 600°C. Experimental data show that this temperature corresponds to the onset of ductile deformation in olivine [*Goetze and Evans*, 1979]. In this case, T_l will occur at ≤3 km in the fault generation zone at fast spreading ridges but at ≤6-8 km in the fault generation zone at slow spreading ridges (see Figures 5 and 6).

The upper stability transition T_u is less well understood. However, two more detailed explanations have been recently put forward. Using an elastic model for the contact between two rough surfaces, *Scholz* [1988*b*] showed that l_c decreases with increasing normal stress and calculated that the transition to unstable sliding occurs above an effective normal stress of 30-40 MPa. *Marone and Scholz* [1988] showed experimentally that thick accumulations of poorly consolidated fault gouge exhibit intrinsically stable sliding, i.e., (a - b) is positive. Unconsolidated fault gouge is usually best developed in the shallow portion of a fault zone and correlates with the amount of displacement on the fault [*Robertson*, 1982]. Bathymetric data indicate that fault scarps on slow spreading ridges can reach heights of 600-800 m or more, which is at least a factor of 3 larger than that observed on ridges with intermediate or fast spreading rates [*Searle*, 1984]. The difference in gouge development that could be inferred from this difference in fault displacement would imply that faults at slow spreading ridges have developed thicker

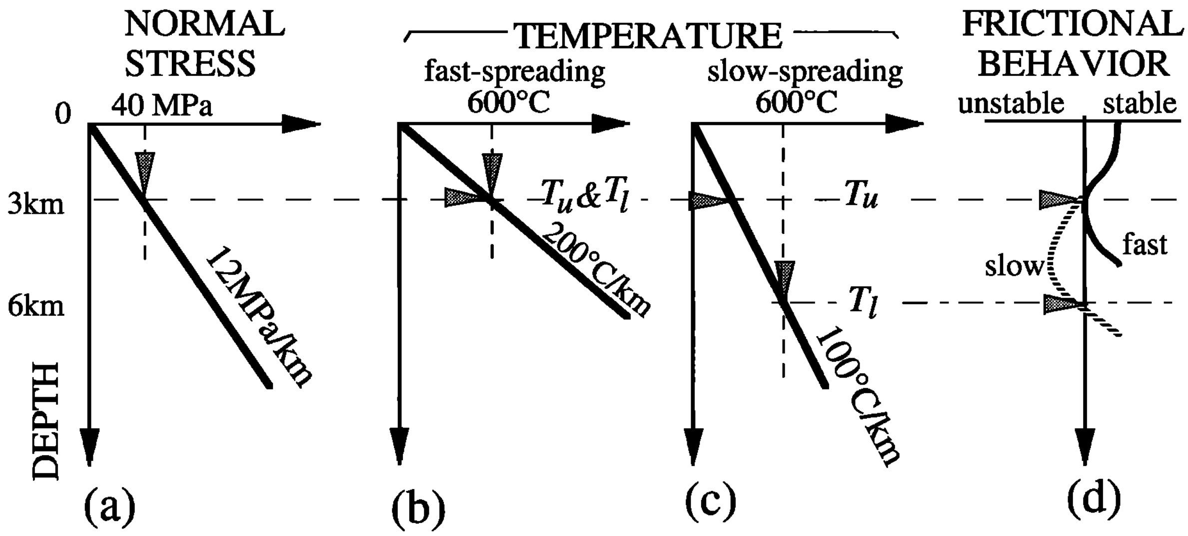

FIG. 5. Frictional stability model for mid-ocean ridge faults. (*a*) Resolved normal stress as a function of depth in the crust for normal faults in the fault generation zone assuming Coulomb friction, hydrostatic pore pressures, a vertical stress of 28 MPa/km, and a fnction coefficient equal to 0.75. (*b* and *c*) Temperature profiles for a fast (100 mm/yr full spreading rate) and a slow (20 mm/yr full spreading rate) ridge, respectively, based on the average thermal structure near the ridge axis [after *Lin and Parmentier*, 1989]. (*d*) Regions of stable and unstable frictional behavior on an active fault at the two different spreading rates. T_u and T_l are the frictional stability transitions controlled by the mean normal stress and the thermal gradient, respectively.

gouge and thus may be more likely to exhibit stable slip. As this is not observed to be the case we investigate instead the effect of normal stress as suggested by *Scholz* [1988*b*]. For extensional faulting the maximum principal stress is vertical and increases with depth in the crust according to $\sigma = \rho g z$, where z is the thickness of the overburden of average density ρ, and g is the acceleration due to gravity. If we assume Coulomb friction with a friction coefficient of 0.75 and a vertical stress increase of 28 MPa/km, then the increase in normal stress with depth in the fault generation zone is 12 MPa/km. Therefore for mid-ocean ridge faults, T_u will occur at about 3 km (Figure 5). We assume here that the position of T_u, which depends on the stress regime, does not vary substantially with spreading rate.

According to this simple model, illustrated in Figure 6, T_l will be coincident with T_u on fast spreading ridges, but close to the ridge axis where the thermal gradient is higher than the average, T_l will most likely be shallower than T_u. Therefore at fast spreading ridges, active faulting occurs in a region dominated by stable slip due to the high thermal gradient (Figure 6). In contrast, on slow spreading ridges there is only a narrow region very close to the axis itself in which T_l is shallower than T_u. As the fault generation zone has finite width, faulting on slow spreading ridges may continue into the region where T_l is deeper than T_u, and in fact T_l and T_u may be quite well separated (Figure 6).

The seismic coupling of oceanic faults χ can be defined by the ratio of the seismic width of the fault, W_s, to the total down dip width of the fault, W_f. The width W_s is controlled by the positions of T_u and T_l, i.e.,

$$W_s = \frac{T_l - T_u}{\sin(\theta)} \qquad T_l > T_u$$
$$W_s = 0 \qquad \text{otherwise.} \tag{11}$$

At fast spreading rates where T_l is at the same depth or shallower than T_u, W_s is zero so that χ equals zero. Although the model described above predicts that W_s is always smaller than W_f, independent of spreading rate, once an earthquake has nucleated, it can rupture the whole fault. This is because the rupture can propagate through the frictional stability transitions, although they will inhibit the propagation. *Solomon et al.* [1988] found that the centroid depth of earthquakes on slow spreading ridges is at about 6 km which is approximately the depth of T_l between about 1 km and 5 km from the axis. The maximum depth of seismic rupture is probably about twice the centroid depth. Therefore at slow spreading rates the effective seismic width W_s, at least for the largest earthquakes, may be comparable to W_f.

The model derived above provides a simple first-order explanation for the observed variation in seismic activity as a function of spreading rate. Hydrothermal circulation at mid-ocean ridges, which often utilizes faults as conduits, may also influence the seismic activity and should be considered. *Reinen et al.* [1991] have found that serpentine, a weathering product of basalt, is characterized by stable frictional sliding ((a - b) positive) over a range of confining pressures for slow loading rates typical of plate motion velocities. These workers conclude that serpentinite should not be the site of instability initiation although propagation of unstable slip initiated on another portion of the fault may be permitted. The flux of fluids and thus hydrous alteration of fault zone materials is probably affected by fault activity, i.e., slip rate. The slip rate on Holocene and Quaternary faults in the slow spreading Asal Rift, Djibouti, measured by *Stein et al.* [1991], is of the order of 1-2 mm/yr. By measuring the width of acoustic shadows in SeaMARC I side scan images collected along the EPR axis near 12°N we have estimated a maximum scarp height of about 120 m for a fault at a distance of 1 km from the axis (see *Crane* [1987] for a description of the original data set). If we assume a dip of 45°, this fault has had an average slip rate of about 8 mm/yr, assuming that it started to form right at the

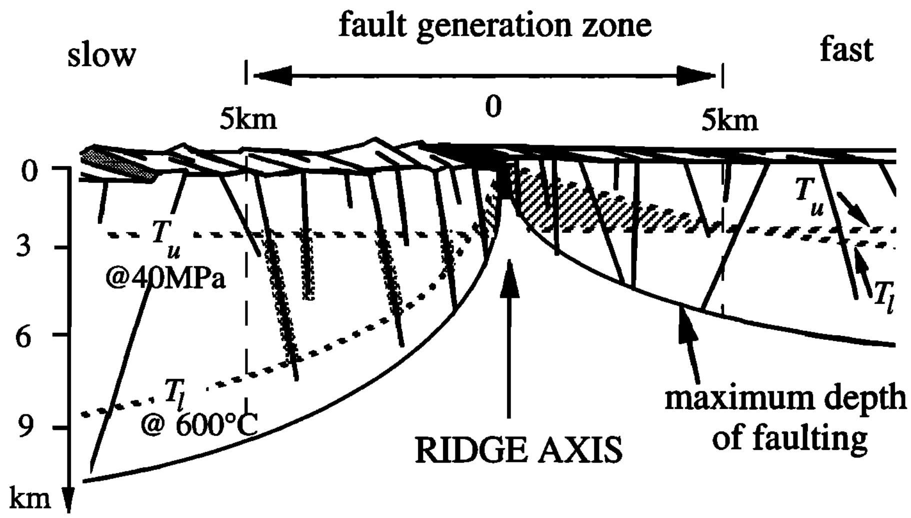

FIG. 6. Cross section through oceanic lithosphere adjacent to the ridge axis according to the frictional model shown in Figure 5. The half-width of the fault generation zone is taken to be 5 km. The left hand side illustrates a slow spreading ridge, and the right hand side illustrates a fast spreading ridge. T_u and T_l are defined in Figure 5. The shaded area indicates the region where $T_l \leq T_u$ so that faults in this region slip stably. The hatched pattern indicates unstable slip on faults at a slow spreading ridge.

axis and was still active when it was imaged. Even if we assume the fault to be vertical at the surface the slip rate would have been 6 mm/yr which is 3-6 times higher than in Asal. It seems reasonable to conclude that fault slip rate (as opposed to accumulated fault displacement) and the thermal structure at the axis may be the important factors determining the seismic characteristics of oceanic faults.

CONCLUSIONS

Using side scan sonar and bathymetric data from the flanks of the EPR at 13°-15°N and near 3°S we have calculated that of the order of 5-10% (with a possible range from 3 to 15%) of the total plate separation rate is achieved by brittle extension of the oceanic crust at the rise axis. The contribution of brittle deformation to seafloor spreading appears to be negatively correlated with spreading rate. Specifically, we calculate that for spreading rates greater than 150 mm/yr, the fault strain $\varepsilon_{xx} \approx$ 3-9%, which is consistent with estimates from independent studies. For spreading rates of about 100 mm/yr we find that $\varepsilon_{xx} \approx$ 5-15%. The only direct estimate of fault strain from the MAR, where the spreading rate is 20 mm/yr, is in the range 11 to 20%. This estimate from the MAR is comparable to calculations of brittle deformation from the seismic moment released during normal faulting earthquakes at the ridge axis. Seismic coupling, which is defined as the ratio of seismic to aseismic slip occurring on a fault, appears therefore to be about 100% on the MAR. In contrast, even if the detection limitations of central Pacific earthquakes are taken into consideration, we calculate that only about 1% of the fault strain on the EPR can be accounted for by seismicity. Therefore the seismic coupling of normal faults on the EPR is virtually zero. The discrepancy between the observed fault strain and the seismicity along the spreading centers of the EPR is explained by a model in which faults at fast spreading ridges slip stably, rather than in a stick-slip fashion, due to the high geothermal gradient. An additional factor may be the flux of hydrothermal fluids along mid-ocean ridge faults, which generates alteration products shown to exhibit intrinsically stable sliding in friction experiments. If fluid flux is controlled by fault activity and thus slip rate, hydrothermal effects may be enhanced at fast spreading ridges where fault slip rates appear to be unusually high.

The results presented here indicate that there are marked differences in the seismic coupling of normal faults forming at mid-ocean ridges with extremes in spreading rate. It remains to be demonstrated how seismic coupling varies gradually over the observed range of slow, intermediate, and fast spreading rates. The next step toward this ultimate goal is a more comprehensive calculation of fault strain at slow spreading ridges than has previously been done. The effect of along-axis variations in fault development, as documented by *Shaw* [1992], should also be examined. Given that large-magnitude earthquakes do occur on the MAR and that the station control is this area is better than for the central Pacific, a detailed comparison of seismicity and faulting should be possible. In this way, we may be able to establish whether some of the faulting is aseismic even at low spreading rates.

Acknowledgments. The authors acknowledge helpful discussions with Neil Mitchell, Dan Fornari, Kim Kastens, and Bill Ryan. Roger Searle generously provided original copies of the GLORIA images near 3°S and unpublished data on fault lengths. We also thank Suzanne Carbotte for many helpful comments and for providing preprints of her work. Marc Parmentier and Eric Bergman provided thorough and helpful reviews which improved the final manuscript. The initial stage of this project was supported by NSF contract EAR90-04534, and it was completed with the support of the Office of Naval Research under contract number N00014-89-J1159.

REFERENCES

Bicknell, J. D., J.-C. Sempere, and K. C. Macdonald, and P. J. Fox, Tectonics of a fast spreading center: A Deep-Tow and Sea Beam survey of the East Pacific Rise at 19°30'S, *Mar. Geophys. Res., 9,* 25-45, 1987.

Blackinton, J. G., D. M. Hussong, and J. G. Kosalos, First results from a combination side scan sonar and seafloor mapping system (SeaMARC II), in *Proceedings of the 15th Annual Offshore Technology Conference, Rep. OTC 4478,* pp. 307-314, Offshore Tech. Conf., Dallas, Tex., 1983.

Carbotte, S. M., and K. C. Macdonald, Causes of variation in fault facing direction in the ocean floor, *Geology, 18,* 749-752, 1990.

Cowie, P. A., and C. H. Scholz, Displacement-length scaling relationship for faults: Data synthesis and discussion, *J. Struct. Geol., 14,* 1149-1156, 1992*a*.

Cowie, P. A., and C. H. Scholz, Physical explanation for displacement-length relationship for faults using a post-yield fracture mechanics model, *J. Struct. Geol., 14,* 1133-1148, 1992*b*.

Crane, K., Structural evolution of the East Pacific Rise axis from 13°10'N to 10°35'N: Interpretations from SeaMARC I data, *Tectonophysics, 136,* 65-124, 1987.

Edwards, M. H., D. J. Fornari, A. Malinverno, W. B. F. Ryan, J. A. Madsen, D. G. Gallo, M. R. Perfit, and A. N. Shor, High resolution swath mapping using Sea MARC II over an intermediate to fast spreading segment of the East Pacific Rise from 13° N to 15° N: Quantitative structural data and implications for the fine-scale tectonic evolution of the mid-ocean ridge crest and flank, in IGARSS 89: in *Proceedings of the 12th Canadian Symposium on Remote Sensing,* Part III, pp 1435-1438, Institute of Electrical and Electronics Engineers, Piscataway, N.J., 1989.

Edwards, M. H., D. J. Fornari, A. Malinverno, W. B. F. Ryan, and J. A. Madsen, The regional tectonic fabric of the East Pacific Rise from 12°50'N to 15°10'N, *J. Geophys. Res., 96,* 7995-8018, 1991.

Ekstrom, G., and P. England, Seismic strain rates in regions of distributed continental deformation, *J. Geophys. Res., 94,* 10231-10257, 1989.

Gillespie, P. A., J. J. Walsh, and J. Watterson, Limitations of displacement and dimension data for single faults and the consequences for data analysis and interpretation, *J. Struct. Geol.,* 14, 1157-1172, 1992.

Goetze, C., and B. Evans, Stress and temperature in the bending lithosphere as constrained by experimental rock mechanics, *Geophys. J. R. Astron. Soc., 59,* 463-478, 1979.

Gudmundsson, A., Geometry, formation and development of tectonic fractures on the Reykjanes Peninsula, Southwest Iceland, *Tectonophysics, 139,* 295-308, 1987*a*.

Gudmundsson, A., Tectonics of the Thingvellir fissure swarm, S.W. Iceland, *J. Struct. Geol., 9,* 61-69, 1987*b*.

Huang, P. Y., and S. C. Solomon, Centroid depths of mid-ocean ridge earthquakes: Dependence on spreading rate, *J. Geophys. Res., 93,* 13445-13477, 1988.

Kawasaki, I., Y. Kawahara, I. Takata, and I. Kosugi, Mode of seismic moment release at transform faults, *Tectonophysics, 118,* 313-327, 1985.

Kleinrock, M. C., R. N. Hey, and A. E. Theberge, Jr., Practical geological comparison of some seafloor survey instruments, *Geophys. Res. Lett.,* 19, 1407-1410, 1992.

Klitgord, K. D., and J. D. Mudie, The Galapagos Spreading Centre: A near-bottom geophysical survey, *Geophys. J. R. Astron. Soc., 38,* 563-586, 1974.

Kong, L. S. L., R. S. Detrick, P. J. Fox, L. F. Mayer, and W. B. F. Ryan, The morphology and tectonics of the MARK area from Sea Beam and Sea MARC I observations (Mid-Atlantic Ridge 23°N), *Mar. Geophys. Res., 10,* 59-90, 1988.

Kostrov, B., Seismic moment and energy of earthquakes, and seismic flow of rock, *Izv. Acad. Sci. USSR Phys. Solid Earth, Engl. Transl., 1,* 23-44, 1974.

Laughton, A. S., The first decade of GLORIA, *J. Geophys. Res.,* 86, 11511-11534, 1981.

Laughton, A. S., and R. C. Searle, Tectonic processes on slow spreading ridges, in *Deep Drilling Results in the Atlantic Ocean: Ocean Crust, Maurice Ewing Ser.,* vol. 2, edited by M. Talwani, C. G. Harrison, and D. E. Hayes, pp. 15-32, AGU, Washington D. C., 1979.

Lin, J., and E. M. Parmentier, Mechanisms of lithospheric extension at mid-ocean ridges, *Geophys. J., 96,* 1-22, 1989.

Lonsdale, P., Structural geomorphology of a fast spreading rise crest: The East Pacific Rise near 3°25'S, *Mar. Geophys. Res., 3,* 251-293, 1977.

Lonsdale, P., and F. N. Spiess, Deep-tow observations at the East Pacific Rise, 8°45'N, and some interpretations, *Initial Rep. of the Deep Sea Drill. Proj., 54,* 43-62, 1980.

Macdonald, K. C., and T. M. Atwater, Evolution of rifted ocean ridges, *Earth Planet. Sci. Lett., 39,* 319-327, 1978.

Macdonald, K. C., and B. P. Luyendyk, Deep tow studies of the structure of the mid-Atlantic Ridge crest near lat 37°N, *Geol. Soc. Am. Bull., 88,* 621-636, 1977.

Macdonald, K. C., and B. P. Luyendyk, Investigation of faulting and abyssal hill formation on the flanks of the East Pacific Rise (21°N) using ALVIN, *Mar. Geophys. Res., 7,* 515-535, 1985.

Macdonald, K. C., and J. D. Mudie, Microearthquakes on the Galapagos spreading center and the seismicity of fast spreading ridges, *Geophys. J. R. Astron. Soc., 36,* 245-257, 1974.

Malinverno, A., Inverse square-root dependence of mid-ocean-ridge flank roughness on spreading rate, *Nature, 352,* 58-60, 1991.

Malinverno, A., and P. A. Cowie, Normal faulting and topographic roughness of mid-ocean ridge flanks, *J. Geophys. Res.,* this issue.

Marone, C., and C. H. Scholz, The depth of seismic faulting and the upper transition from stable to unstable slip regimes, *Geophys. Res. Lett., 15,* 621-624, 1988.

Rea, D. K., Model for the formation of topographic features of the East Pacific Rise crest, *Geology, 3,* 77-80, 1975.

Reinen, L.A., J. D. Weeks, and T. E. Tullis, The frictional behavior of serpentine: Implications for aseismic creep on shallow crustal faults, *Geophys. Res. Lett., 18,* 1921-1924, 1991.

Riedesel, M., J. A. Orcutt, K. C. Macdonald, and J. S. McClain, Microearthquakes in the Black Smoker Hydrothermal Field, East Pacific Rise at 21° N, *J. Geophys. Res., 87,* 10613-10623, 1982.

Robertson, E. C. Continuous formation of gouge and breccia during fault displacement, in *Issues in Rock Mechanics, Proceedings of the 23rd Symposium on Rock Mechanics,* edited by R.E. Goodman and F. Hulse, pp. 397-404, American Institute of Mining Engineering, pp.397-404, New York, 1982.

Scholz, C. H., The brittle-plastic transition and the depth of seismic faulting, *Geol. Rundsch., 77,* 319-328, 1988*a*.

Scholz, C. H., The critical slip distance for seismic faulting, *Nature, 336,* 761-763, 1988*b*.

Scholz, C. H., *The Mechanics of Earthquakes and Faulting,* Cambridge University Press, New York, 1990.

Scholz, C. H., and P. A. Cowie, Determination of geologic strain from fault slip data, *Nature, 346,* 837-839, 1990.

Searle, R., GLORIA survey of the East Pacific Rise near 3.5°S: Tectonic and volcanic characteristics of a fast-spreading mid-ocean ridge, *Tectonophysics, 101,* 319-344, 1984.

Shaw, P. R., Ridge segmentation, faulting and crustal thickness in the Atlantic Ocean, *Nature, 358,* 490-493, 1992.

Solomon, S. C., P. Y. Huang, and L. Meinke, The seismic moment budget of slowly spreading ridges, *Nature, 334,* 58-60, 1988.

Stein, R. S., P. Briole, J-C. Ruegg, P. Tapponnier, and F. Gasse, Contemporary, Holocene and Quaternary deformation of the Asal Rift, Djibouti: Implications for the mechanics of slow spreading ridges, *J. Geophys. Res., 96,* 21789-21806, 1991.

Tse, S., and J. R. Rice, Crustal earthquake instability in relation to the depth variation of frictional slip processes, *J. Geophys. Res., 91,* 9452-9472, 1986.

Tyce, R. C., Deep seafloor mapping systems—A review, *Mar. Tech. Soc. J., 20*(4), 4-16, 1986.

Walsh, J. J., J. Watterson, and G. Yielding, The importance of small scale faulting in regional extension, *Nature, 351,* 391-394, 1991.

Wesnousky, S. G., C. H. Scholz, K. Shimazaki, and T. Matsuda, Earthquake frequency distribution and the mechanics of faulting, *J. Geophys. Res., 88,* 9331-9340, 1983.

Wiens, D. A., and S. Stein, Intraplate seismicity and stresses in young oceanic lithosphere, *J. Geophys. Res., 89,* 11442-11464, 1984.

Wilcock, W. S. D., G. M. Purdy, S. C. Solomon, D. L. DuBois, and D. R. Toomey, Microearthquakes on and near the East Pacific Rise, 9°-10°N, *Geophys. Res. Lett., 19,* 2131-2134, 1992.

Wysession, M. E., E. A. Okal, and K. L. Miller, Intraplate seismicity of the Pacific Basin, 1913-1988, *Pure Appl. Geophys., 135,* 261-359, 1991.

P. A. Cowie, Department of Geology and Geophysics, Edinburgh University, West Mains Road, Edinburgh, EH9 3JW, UK.

M. Edwards, SOEST, University of Hawaii at Manoa, Honolulu, HI 96822.

A. Malinverno, Schlumberger-Doll Research, Old Quarry Road, Ridgefield, CT 06877.

C. H. Scholz, Lamont-Doherty Earth Observatory, Palisades, NY 10964.

(Received October 13, 1992;
revised May 27, 1993;
accepted June 8, 1993.)